POLITEHNICA UNIVERSITY OF BUCHAREST

Doctoral School of Electronics, Telecommunications and Information Technology

Decision no. 1047 from 10-07-2023

Ph.D. THESIS SUMMARY

Dipl. Eng. Cosmin-Alexandru IORDACHE

CONTRIBUȚII ÎN DOMENIUL SISTEMELOR INTEGRATE DE TESTARE A COMPONENTELOR ȘI DISPOZITIVELOR ELECTRONICE

CONTRIBUTIONS IN THE FIELD OF INTEGRATED TESTING SYSTEMS OF ELECTRONIC COMPONENTS AND DEVICES

THESIS COMMITTEE

Prof. Dr. Ing. Gheorghe BREZEANU Politehnica Univ. of Bucharest	President
Prof. Emerit Dr. Ing. Mircea BODEA Politehnica Univ. of Bucharest	PhD Supervisor
Prof. Dr. Ing. Claudius DAN Politehnica Univ. of Bucharest	Referee
Conf. Dr. Ing. Marius NEAG Technical Univ. of Cluj-Napoca	Referee
Conf. Dr. Ing. Henri COANDĂ Valahia Univ. of Targoviste	Referee

BUCHAREST 2023

Contents

Chapter 1

Introduction

1.1 Presentation of the field of the doctoral thesis

Now adays integrated testing systems used to test active and passive electronic components exhibits a continuous development. They have been first developed in the same time with first vacuum tubes from the beginning of XX century. During the first world war there were used first tube testers on the battle fields by radio stations operators.

As the components technology has been improved so their applications got wider, a series of parameters have been defined in order to characterize electronic components performances. Increased number of the parameters corresponding to electronic components led to well defined ranges where these devices could work for a specific amount of time guaranteed by their manufacturers.

A testing system for electronic vacuum tubes dated to second world war was made of multiple power supplies, signal generators, voltmeters, amperemeters, an oscilloscope. All of these were consuming a lot of space because of their high volumes, besides this they requested highly trained skills to operated them and also high amounts of electric power. [3]

Few years later, after transistors appeared and been introduced in mass production, these measurement devices used to characterize electronic components start to decrease their sizes, including more and more ways of testing passive and active components.

During next years that came after integrated circuits are born and become more and more popular, with their evolution computers performances are increasing and their dimensions are decreasing. By the end of the seventh decade the American company „Hewlett Packard" has patented its own communication standard for short distances named HP-IB. Laboratory measurement gear manufacturers will use these digital communication networks on short distances in order to speed up the automated measurements processes. This is offering high testing capabilities of electronic components. This standard receives the name of GPIB being the first main standard of digital communication on short distances for measurement gears, it is known also as IEEE-488 starting with 1975 or after 1980 as IEEE-488.1. It allows interconnection of

maximum 15 devices on an 8 bits wide parallel bus that can communicate between them at a maximum speed of 1Mb/s and the maximum recommended distance is 20m. [6]

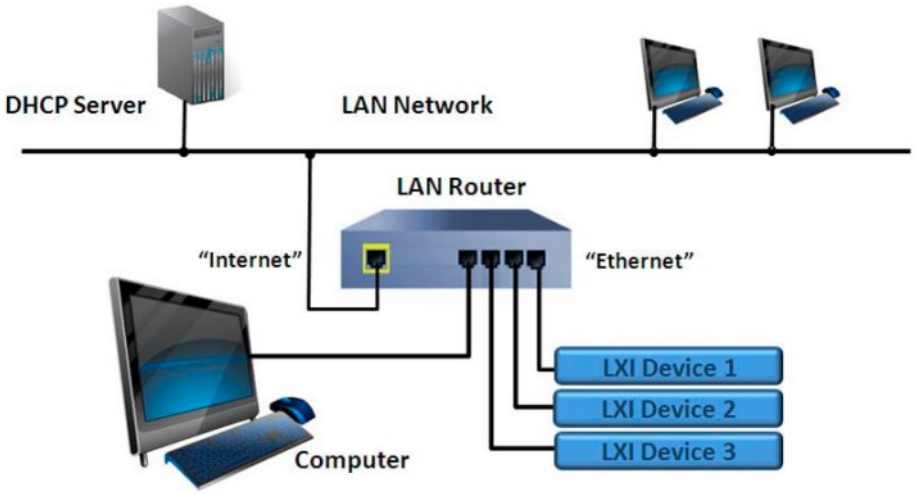

Figure 1.1.2 *Modern integrated and isolated measuring system using LXI [7]*

Computer systems evolved and have been improved, they are using in the present a different type of a much faster communication protocol, compatible with actual high-speed buses. This is named LXI and besides high speed it offers the possibility to interconnect a higher number of instruments than GPIB. It can reach transfer speeds up to 1Gb/s and communication between measuring instruments is much easier. [8]

Several laboratory measurement gear from the present besides LXI have the option to communicate on an USB port. This way of communication is at least the same as popular as the LAN, it is used mainly where there are few instruments interconnected and the distance between them and the host is relatively small. Integration costs of an USB interface are smaller compared to a LXI interface because of the wider spread of the USB protocol also used on large scale. [9]

Actually, electronic components manufacturers are offering SPICE models to clients for almost any device or even module part of their portfolio. This is already an industry standard and the complexity of these SPICE models is continuously growing.

1.2 Scope of the doctoral thesis

The scope of this philosophy doctoral thesis is coming with a series of contributions into integrated testing systems of electronic components and devices with low currents and low to medium voltages, covering a wide range starting with electronic vacuum tubes up to JFET, MOSFET or IGBT transistors or linear integrated circuits. This paper presents a detailed characterization of electronic vacuum tubes.

The main objective it is represented by developing a prototype that can perform a I(V) characteristic of a device using pulsed measurements, this way allows to go over maximum recommended power without damaging the electronic component.

The novelty in this domain is the implementation of such technique and building up of a testing system starting with the USB interface to a personal computer that could display in real time the measurements and store them for future extraction of SPICE model coefficients extraction. In this way a more accurate SPICE model can be issued for the device under test and simulations results will become more accurate leading to a better digital environment replica of the real electronic circuit.

For example, developing an audio frequency amplifier with electronic tubes starts from a first SPICE simulation done in a virtual environment to verify concept schematics and determine preliminary amplifier's performances. Such a simulation is based on the presumption of a correct and complete SPICE model of the electronic components used, also valid for the vacuum tubes' models.

I have built such a high-fidelity audio frequency amplifier for my bachelor of science degree thesis where the accuracy of tubes' SPICE models had a strong contribution to validate the concept and to adjust adjacent components' dimensions.

1.3 Contents of the doctoral thesis

This philosophy doctoral thesis consists in 5 chapters as it follows:

Chapter 1 is an introduction in the domain of integrated measurement and control systems, it contains the motivation of this thesis.

Chapter 2 presents in detail an original solution implemented up to a prototype level regarding the curve tracer development with pulsed measuring option for electronic vacuum tubes. It begins with the analog section and continues with the numerical one, their testing and the dedicated software interface for Windows operating systems.

This curve tracer can be integrated in a complex measurements system because of its USB connection, in this manner it can operated from distance.

Chapter 3 presents a new solution of suppling the vacuum tubes heaters. Low voltage power supply has been improved by increasing its power, its speed of reaction and its energy efficiency.

Chapter 4 presents in the first part actual SPICE models for electronic tubes. In the second part there are presented the results of coefficients extraction corresponding to a SPICE model of an electronic tube characterized with the prototype from 2nd chapter.

After these coefficients determinations there will be compared the SPICE model versus the real characteristic of the device under test.

Chapter 5 contains the conclusion of this thesis, the contributions in prototype development from the second chapter and afterwards developments followed by coefficients extractions and in the final future development ideas and public papers list.

Chapter 2

Integrated characterization system of electronic components

For SPICE models coefficients extraction for an associated electronic device or any active electronic component it is necessary a very good characterization of that device or component.

In the past coefficients extraction was done using tubes or transistors datasheets charts or having discrete static measurements in different successive operating points but without running over maximum recommended dissipated power.

There are tubes or transistors whom current-voltage characteristics do not have a very good resolution neither in the datasheets or in catalogs and in this case, there is a need to trace these characteristics with a very good resolution to make possible exact SPICE models coefficients extraction.

2.1 System architecture and basic specifications

Developing of this characterization system for active electronic components is based on its compatibility with today's computing systems. So, the decision of using an USB interface appeared because of the popularity of this protocol and its spread in actual measurements systems.

Pulsed characterization of semiconductor devices or electronic tubes over their recommended maximum dissipation area pretends a complex system of controlled power supplies with a very fast transient response. Beside this the system should offer the possibility to measure and data log the voltages and currents present on the devices under test pins.

An electronic tube it is made from a cathode and one or more grids with one or more anodes [14]. The majority of electronic tubes can be tested with a minimum of four independent controlled power supplies. The system with four independent controlled power supplies can be used also to characterize transistors or diodes, silicon-controlled rectifiers, diacs or resistors, capacitors and many other passive or active components.

In this thesis I will present in details characterization of an electronic vacuum tube followed by a SPICE model coefficients extraction and its testing in a virtual simulation environment.

Basic specifications of the CCTracer [15] system start with voltages and currents ranges associated to controlled power supplies. In the way of an output characteristic extraction for a vacuum tube, for example a triode, it is needed a power supply for the heater, another one between control grid and cathode and the third one for the anode.

Heater power supply should deliver a tunable voltage between 0 V and 30 V (with a setting voltage precision of 5%) within a range of currents starting from 50 mA up to 3 A, having an overcurrent protection that limits the output current fed to the device under test. This range of voltages covers the majority of electronic tubes starting from 1,2 V, 5 V, 6,3 V, 12,6 V or 24 V up to 30 V included.

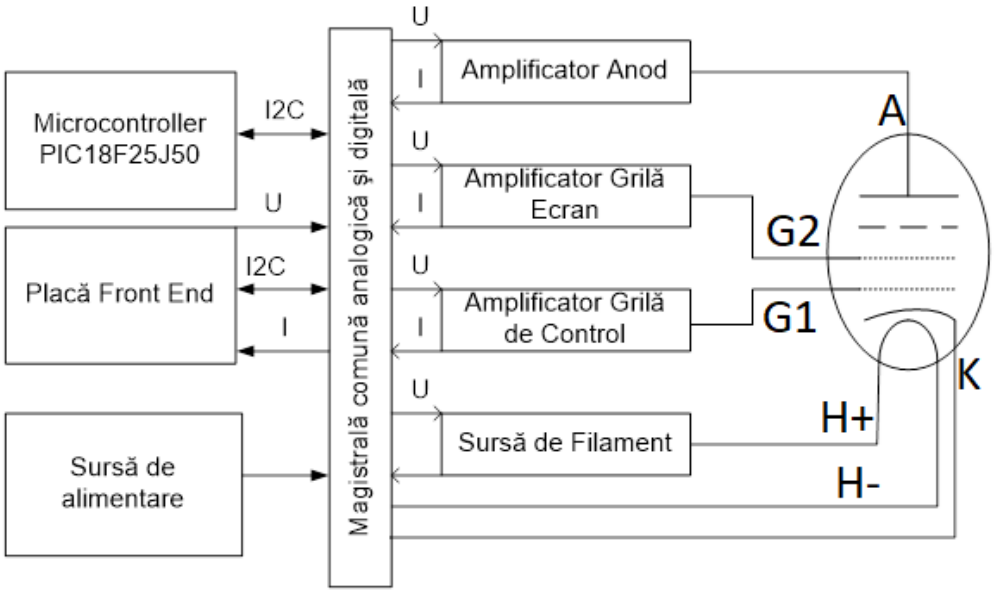

***Figure 2.1.1**. Electronic tubes characterization system concept schematic*

Next variable **power supply** used for the **control grid** of an electronic tube will have 2 ranges, first range A from 0 V up to 30 V and second B from - 100 V to 0 V (with a voltage setting accuracy of 0.1 %), the possibility to measure the grid current with and accuracy of 0,1 % and a fast transient response of maximum 100 us on both ranges.

For **the anode or screen greed the power supply** should offer a voltage between 0 V and 400 V (with a voltage setting accuracy of 0.5 %) having a fast transient response of maximum 100 us and the possibility of current measurement in the range of 0 mA ÷ 500 mA with an accuracy of 0,1 %.

This system of variable controlled power supplies will be interconnected with a microcontroller with **USB support** together with a personal computer, afterwards the possibility of user assisted calibration using only **the software interface** will be integrated into **dedicated software**, designed in Visual Basic.

Block schematic was designed so as to offer a simple and precise way of current measurement. Because of this, digital ground is not at the same potential as the device under test ground, between them there is a 410 V shift.

2.2 Amplifiers design

2.2.1 Anode amplifier

The anode amplifier's concept is presented in figure 2.2.1 , driving voltage is applied on the input of U2 operational amplifier through R4 resistor. U4 amplifier drives the PNP transistor Q2 so this transistor will act like a voltage to current converter.

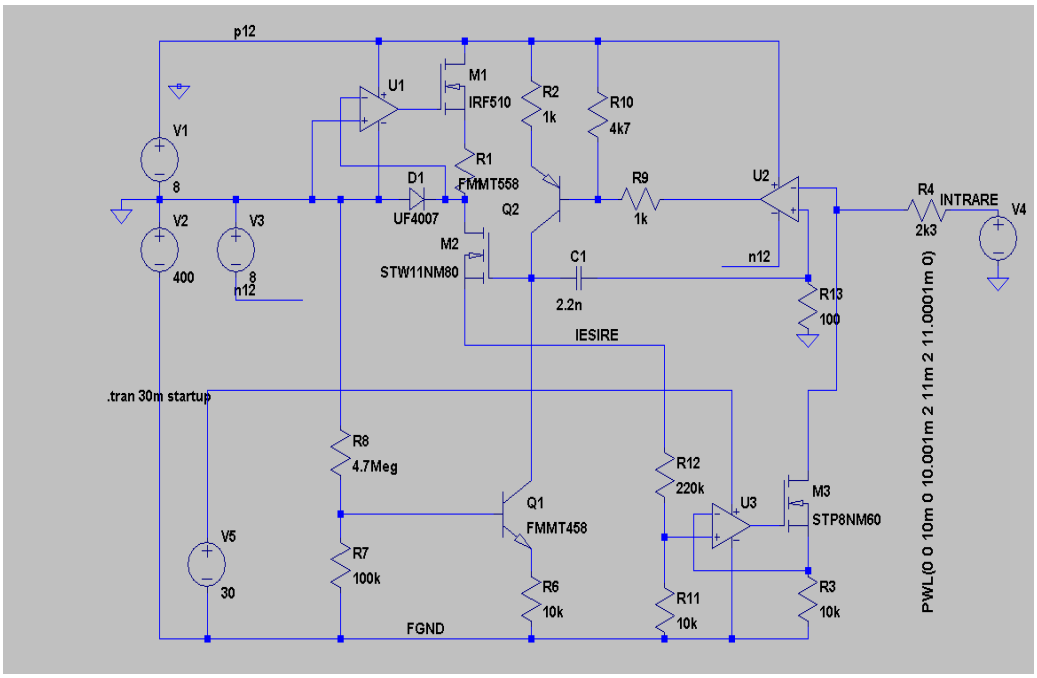

***Figure 2.2.1**. Anode amplifier concept schematic*

Q2 transistor has its collector biased by Q1 constant current source. Q2 drives the source repeater M2 MOS transistor's gate, M2's source is also the output of this stage.

From the output the voltage is decreased by R11-R12 divider and applied to the M3 - U3 voltage to current converter. The current generated in M3's drain is provided to the input node which is the noninverting input of the operational amplifier U3. The capacitor C1 together with R13 resistor are part of the compensation network of the amplifier, by introducing a low frequency dominant pole.

Constant current source U3 - M3 behavior is described by the following equation:

$$I_{D,M1} = V_{OUT} \cdot \frac{R11}{R11 + R12} \cdot \frac{1}{R3} \qquad (2.2.1)$$

In a static regime, the output voltage will be set if this current from eq. (2.2.1) it is equal to the input current:

$$\frac{(V_{IN} - DGND)}{R4} = I_{D,M1} = V_{OUT} \cdot \frac{R11}{R11 + R12} \cdot \frac{1}{R3} \qquad (2.2.2)$$

So the output voltage V_{OUT} equation will be:

$$V_{OUT} = (V_{IN} - DGND) \cdot \frac{R3 \cdot (R11 + R12)}{R4 \cdot R11} \quad (2.2.3)$$

In this way it is also obtained a level shift of the signal, starting from the analog ground (of ADC and DAC converters) towards to the floating ground FGND, which is set to – 400 V below the digital ground.

The components out of this equation have been sized to conduct to a closed loop gain of 100.

$$V_{OUT} = 100 \cdot (V_{IN} - DGND) \quad (2.2.4)$$

Current measurement is done with U1 operational amplifier, M1 transistor and R1 resistor.

Transient response simulation has been done with a 2 V input pulse having a length of 5 ms and targeted output voltage is 200 V referenced to floating ground FGND, pictured in figure 2.2.2 .

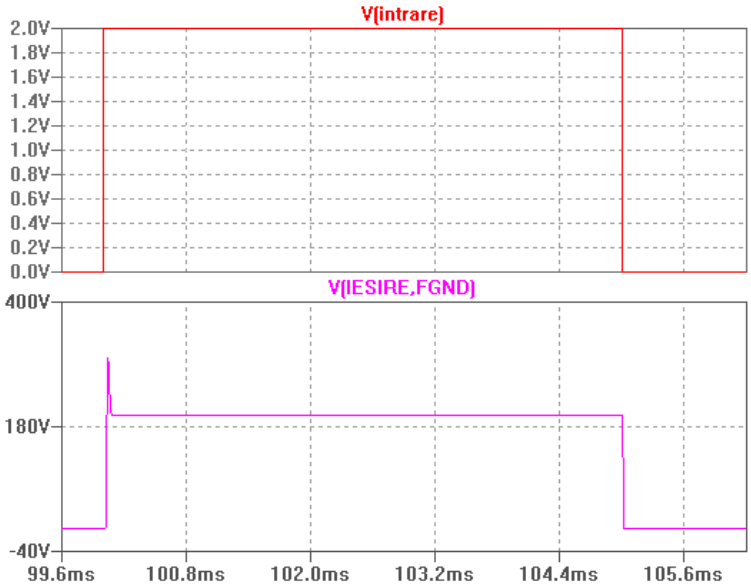

Figure 2.2.2. *Input voltage (red) and output voltage (purple)*

In figure 2.2.3, on the rising edge, it can be seen that target voltage is already set after 33 us. After this time range, voltage continues to grow, having an overshot of 40 % out of targeted voltage. Output voltage then settles down to programmed value after another 57 us.

On the falling edge in figure 2.2.4 the voltage is decreasing faster, in approximately 15 us.

2.2.2 Screen grid amplifier

The amplifier of the screen grid is identical to the anode one presented in the previous subchapter. It can be used in the same time with the anode amplifier to test simultaneously a double triode or double diode.

2.2.3 First grid amplifier for negative voltages

The amplifier of control grid has to provide both positive and negative control voltages, referenced to the floating ground. So, I have designed two different amplifiers and their outputs will be switched with a relay when they reach 0 V.

This amplifier in order to deliver down to – 100 V on the control grid of the device under test will have a gain of approximately 100, driven by a control voltage (sourced from a numeric to analog converter).

In the concept schematic from figure 2.2.9 the first grid amplifier is driven by V6 source through R4 resistor present to the input of operational amplifier U2.

The output of this operational amplifier opens Q4 transistor. It will drive M1, connected to a minus 500 V potential. In order not to stress Q4 over its maximum allowed collector-emitter voltage it was introduced PNP transistor Q3. It is a common base which is not contributing to current amplification of the circuit. Collector current of Q4 produces a drop voltage on R6, this voltage drop drives M1 mosfet transistor.

Operational amplifier U1 together with M3 mosfet transistor will maintain a virtual zero voltage on the source of M3. In this way the voltage in this node will be equal to the voltage of the floating ground. Diode D1 acts like a protection in order to avoid leaving the floating node to decrease too much and to endanger the operational amplifier U1.

The current through R1 resistor will pass through M3 source terminal and then it will reach the inverting input of U2, if the currents are being equalized, equation (2.2.3.1) is met.

$$I_{R1} = I_{R4} \tag{2.2.3.1}$$

The voltage level at inverting input of U1 is zero, being equal to the voltage on the noninverting input. Also, the voltage on R1 is referenced to the floating ground having the same potential with the cathode of the device under test. Considering V_{IN} = V(IN)-V(0) while V_{OUT} = V(OUT)-V(FGND).

$$\frac{V_{IN}}{R4} = -\frac{V_{OUT}}{R1} \tag{2.2.3.2}$$

The gain of the circuit is equal to the ratio of R1 and R4, more exactly, the gain is 100 K / 1 K = 100. So, the maximum negative voltage that can be applied to the first grid is – 100 V when the on the input is applied 1 V.

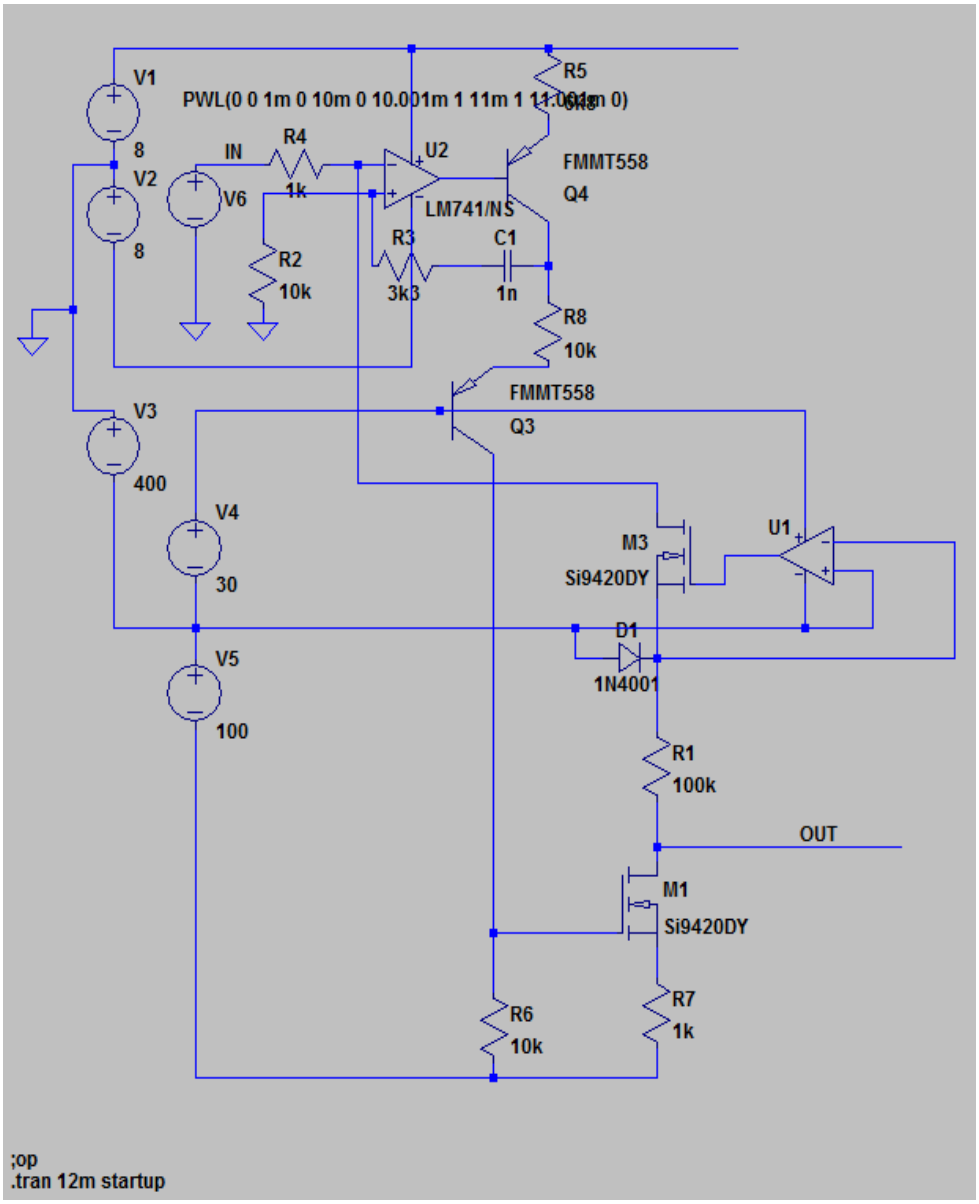

***Figure 2.2.9**. Negative voltages first grid amplifier concept schematic*

For simulation purposes, on the input was applied a pulse of 0.5 V, at the output will get a pulse of -50 V like in figure 2.2.10.

When a positive transient voltage is applied on the input then the output starts to decrease. After 64 us it will reach targeted voltage followed by a 20 % overshoot. After another 90 us the output settles to the programmed voltage. This translates to a relatively small phase margin of the amplifier, considered to ensure a fast transient response for a given input pulse.

For a negative voltage transient, the output voltage is discharging and ramps up to FGND in no more than 40 us.

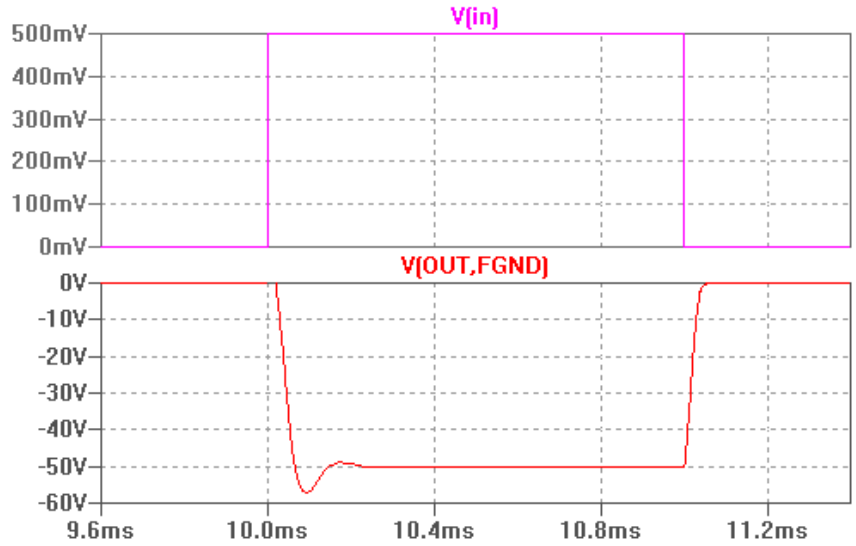

Figure 2.2.10. *Simulation of negative voltages G1 amplifier*

2.2.4 First grid amplifier for positive voltages

The first grid amplifier for positive voltages was designed similary to the anode amplifier. Its concept is the same but the maximum output voltage is lower, only 30 V.

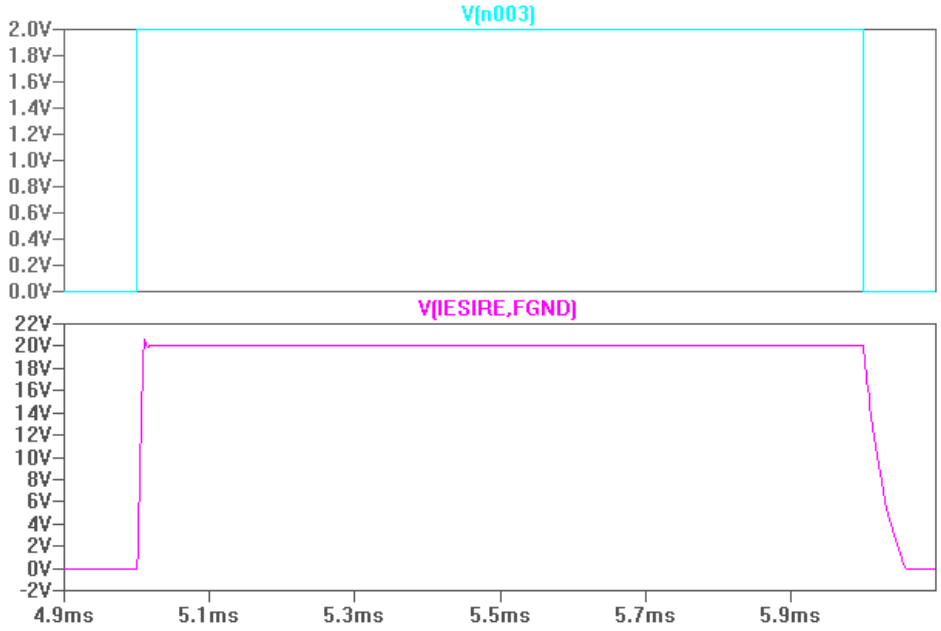

Figure 2.2.12. *Simulation of positive voltages G1 amplifier*

In the simulation from figure 2.2.12 it was applied a 1 ms pulse on the input with an amplitude of 2 V. As consequence at the output there will be a pulse with the same width but with a 10 times higher amplitude.

For a positive transient, the output settles in no more than 13 us with a small overshoot while for a negative transient the output is discharged by the load resistor in no more than 60 us.

2.3 Heater power supply design

The power supply concept used for the heater or the heaters can be split into two sections: first one is the level shifter and the second one is the hysteretic buck converter. For efficiency reasons I've decided to use a switching mode voltage down converter.

Starting with the level shifter, this receives a control voltage referenced to the digital ground level and delivers at the output a 10 times bigger voltage referenced to the floating ground. There is a voltage to current convertor built with Q1 transistor together with U3. Generated current, proportional to V(VIN) is applied to resistor R4. In this way there is obtained a voltage amplification in a range given by the ratio of R4/R2.

This voltage is used as a reference for the second section of the schematic, the buck converter. In parallel with R4 resistor there is a 100 nF capacitor which ensures a smooth voltage transient and also a soft start of the power supply.

The reference voltage is applied to U2 comparator input, which has a hysteresis defined by R3. The output of the comparator drives the power transistor M1 with the totem pole formed of Q3 & Q4 transistors, connected as buffers.

The power stage of the buck converter is built with the coil L1, diode D2 and transistor M1. In series with the C1 capacitor was added an artificial ESR with resistor R7. This ESR is essential for a proper working of every hysteretic converter, because this additional ESR produces a voltage ripple which will be propagated to the feedback network. Negative feedback for the voltage regulation is set by R10.

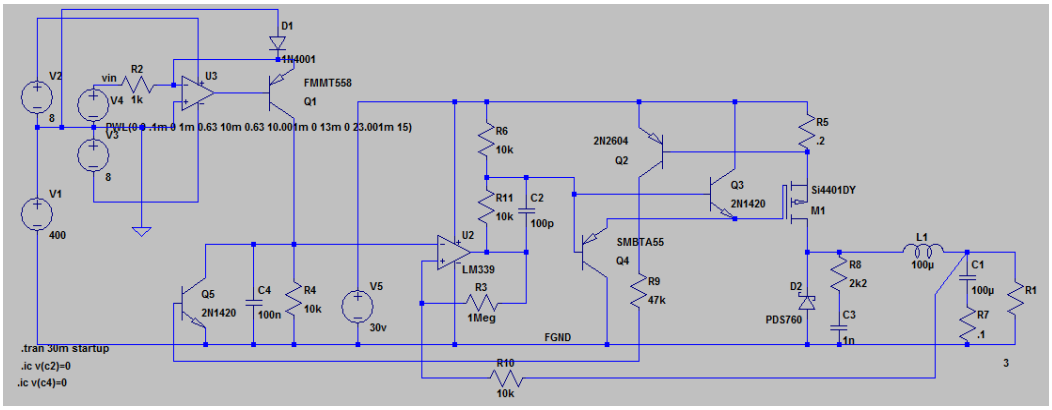

***Figure 2.3.1**. Heater power supply concept schematic*

Overcurrent protection of the converter is done by R5 and Q2. When a bigger current is passing through R5 then Q2 turns on and its collector current is applied on the base of Q5. So, Q5 turns on and the reference voltage is decreasing. When the overcurrent is gone then Q2 and Q5 are off and the reference comes back to its previously set voltage.

Heater power supply simulation was done assuming a 3 Ω resistive load and an output voltage of 6.3 V. For this purpose, the input voltage was set to 0.63 V, in figure

2.3.2 it is presented the startup waveform and in figure 2.3.3 the voltage on L1 and filtering capacitor C1 internal current shape.

In constant voltage mode, TON and TOFF switching periods are leading to a current ripple through capacitor C1. This current ripple translates to a voltage ripple on resistor R7, which is going through the negative feedback network down to the noninverting input of the comparator circuit.

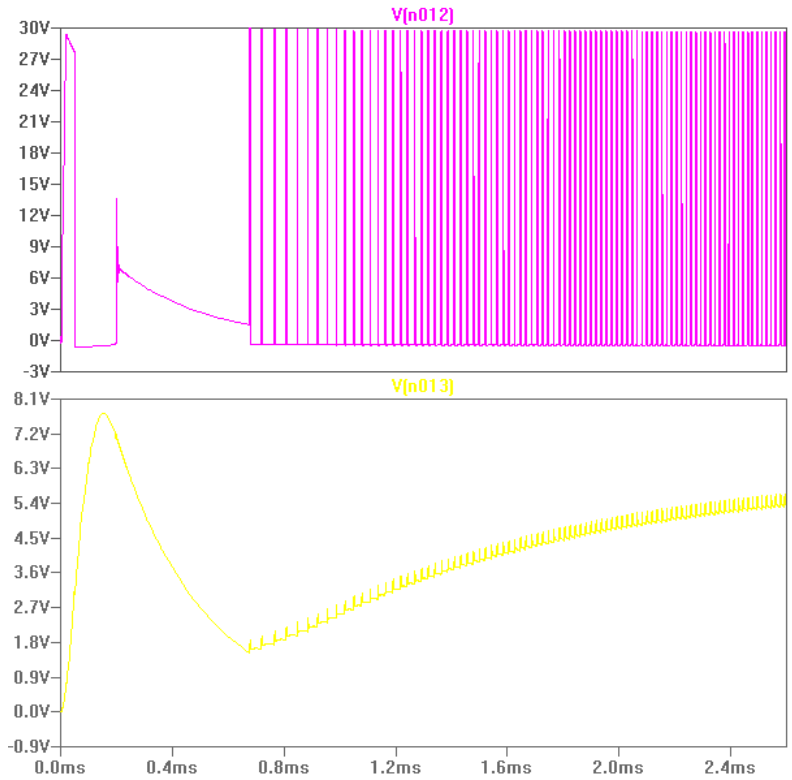

Figure 2.3.2. *Startup of the heater power supply – the voltage on the M1 source pin (pink) and the output (yellow)*

2.4 Analog to digital and digital to analog interfaces

Analog to digital and digital to analog interfaces are setting the references for the analog amplifiers, and reads the analog values of the currents through those 3 pins of the device under test: anode current, screen grid current and first grid current corresponding to positive voltages. The microcontroller is communicating through an I2C bus with the Analog to digital and digital to analog converters. [18]

2.5 Control module

This control module is built around PIC18F25J50 [21] microcontroller. On the same board of the module there can be found the circuits that are highlighting any overcurrent to the microcontroller as well as the circuits that are preconditioning the measured voltages so they can be measured safely with the internal ADC. [18]

2.6 Protections

Device under test pins are connected to the internal circuitry of the tracer by the help of relays. These relays are isolating the device under test in case of an overcurrent or an overvoltage on its leads, or if the tracer is off or in stand-by.

2.7 Power supply

All the blocks presented previously were tested in the lab using many power supplies. The integrated characterization system of electronic devices in order to work independently it has to have a proper power supply compatible with the single-phase public electricity transportation network.

For this purpose, I've decided to use a linear power supply to benefit of a lower noise and easy debug if needed. The power supply consists of a high-profile toroidal transformer of 200 W, silicon diode rectifiers and filtering capacitors on each rail. Low voltage rails contain linear voltage regulators connected in series, part of the family 78xx and 79xx, more exactly 7805, 7805 and 7908.

2.8 Motherboard

The interconnection board named also the mother board is the way that all those 7 boards are connected together. This motherboard has 7 ISA sockets and more small bolts connectors used to tie the cables.

The signals present on the motherboard are presented in the table 2.8.1.

2.9 Prototype design

Electronic boards of the system were designed to fit in a Metroset enclosure measuring 30 cm x 15 cm x 35 cm.

In figure 2.9.1 is illustrated the arrangement of the internal boards.

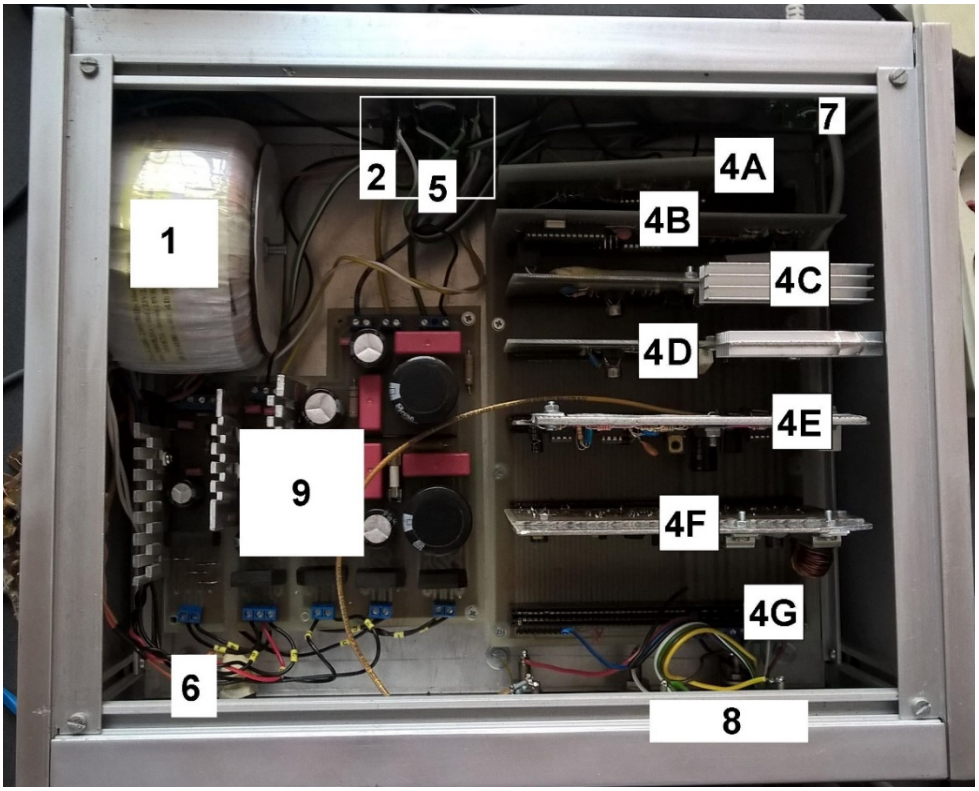

Figure 2.9.1. *Mechanical placement of the boards*

Table 2.9.1*. Working sub-blocks list*	
1	Toroidal power supply transformer
2	Fuses panel
3	Motherboard
4	Working boards
5	Power supply outlet interconnection
6	Power switch
7	USB connector
8	DUT connectors
9	Power supply

On the motherboard there are interconnected the working boards. They are presented in table 2.9.2 starting from the back of the enclosure up to front panel.

Table 2.9.2*. Working boards list 4A÷4G*	
Board A:	Analog to digital and digital to analog converters board
Board B:	Microcontroller board

Board C:	Anode amplifier board
Board D:	Screen grid amplifier board
Board E:	G1amplifier board
Board F:	Heater power supply board
Board G:	Relay protections board

2.10 Graphical user interface

This graphical interface was developed initially in Microsoft Visual Studio 2010 Express [15], [18] in version 1.0. It consists of a main window with 2 sub-menus which lead to saving or opening a set of measurements or straight to the software calibration menu or the sanity check of internal power supplies voltage levels.

I have generated a new program version for 64b processors. Besides this I've improved the graphics of the legend section from the main window, also I've added each axe measurement units.

The main window architecture, it has on the left side a legend and I(V) graphic while on the right side the number of steps needed for the maximum value of anode voltage, also control grid voltage steps and their number. Also for tetrodes or pentodes screen grid voltage level can be set together with the maximum current level allowed.

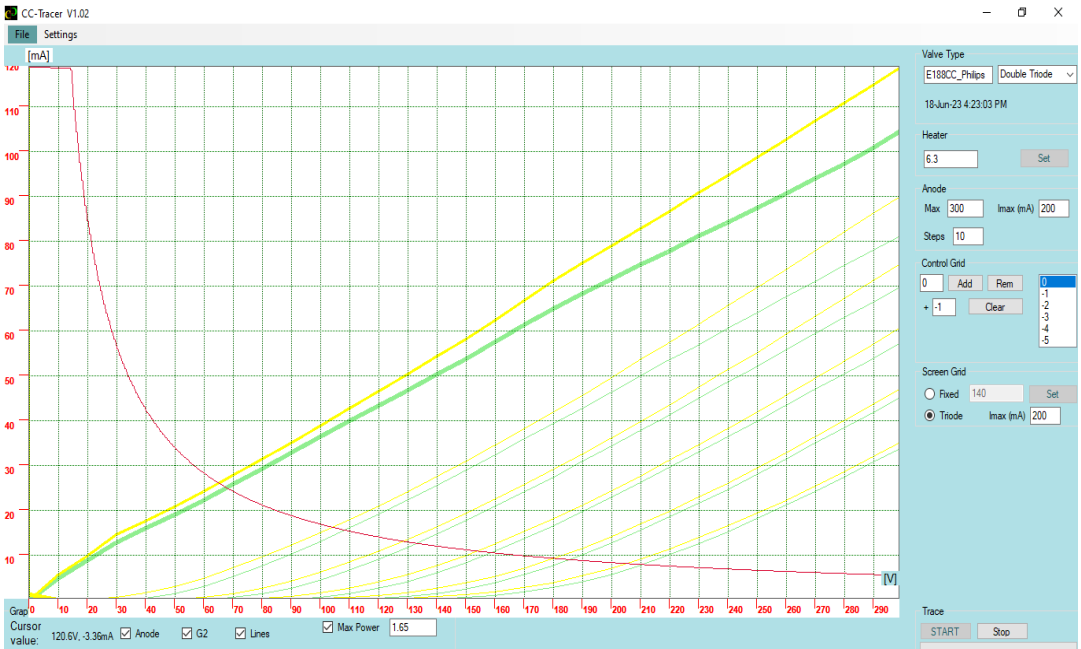

Figure 2.10.3. *Extended output characteristic of a double triode E188CC Philips*

In the figure 2.10.3 it can be observed the extended output characteristic of a double triode E188CC Philips, according to the datasheet [24] it has a maximum anode dissipated power allowed of 1,65 W and the pulse measurements made it possible to go over the maximum power curve (pink curve from figure 2.10.3) in the highest point of the graph of about 20 times, which means 33 W.

Chapter 3

High efficency heater power supply

Power demands inside the majority electronic equipment, starting with the portable ones and up to the automotive or industrial ones, need a high efficiency conversion. Recent trends in the digital management of the energy have gained higher attention, especially regarding dc-dc small or medium power converters. [25].

So, for a high efficiency in a small and compact volume such is CCtracer I've decided to build a switching converter. It will have a bigger power compared to the previous one in sub-chapter 2.3 of this thesis but it should fit into the same area of the pcb.

3.1 Concept of current mode buck converter

Switching converter buck with current control mode (CMC) has the advantage of overcurrent selfprotection, a better stability, a faster transient response compared to other voltage controlled converters [26].

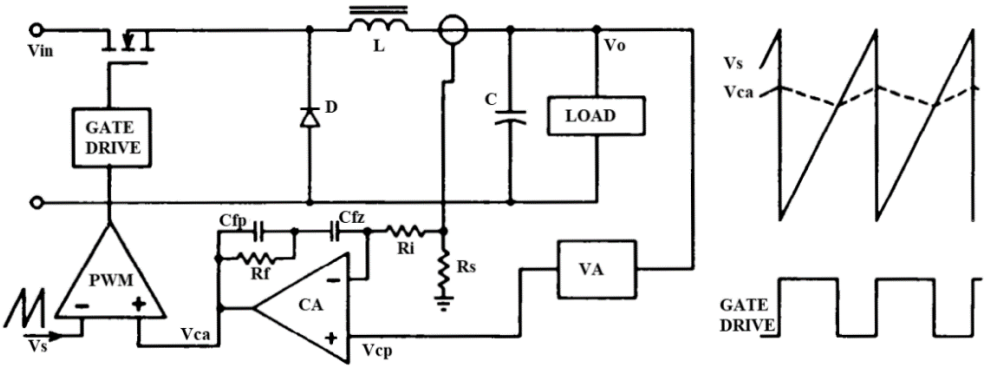

Figure 3.1.2. Concept schematic of a switching converter with a control loop based on the average coil current

3.2 Current mode buck converter design

The switching down converter will be integrated into CCtracer to supply tube heaters or to serve as a variable power supply for other devices under test. It will have a voltage range of 1,5 V ÷ 40 V and a maximum current of 7,5 A. In total the convertor will deliver to maximum load about 300 W. Working input voltage level will be 48 V.

The switching power supply will be controlled by the circuit LT 3724. [28] According to the datasheet the working frequency is 200 KHz. Starting from this value and taking into account eq. (3.2.1) for an output voltage V_{OUT} = 30V, a maximum allowed input voltage $V_{IN(MAX)}$ = 50 V, a current ripple ΔI_L = 20% then the inductance value of the coil should be L ≥ 40 µH.

Taking into account the maximum output current value of 7,5 A and the internal current comparator threshold fixed to 150 mV will lead to a shunt resistor of 20 mΩ. After these preliminary calculations, a possible solution for the coil is [29] an inductor with L = 47 µH and an internal resistivity of 19,2 mΩ.

Following the concept schematic inside the datasheet of the control circuit LT 3724. [28] the minimum value of the inductor L could be obtained with eq. (3.2.1):

$$L \geq V_{OUT} \cdot \frac{V_{IN(MAX)} - V_{OUT}}{f_{SW} \cdot V_{IN(MAX)} \cdot \Delta I_L} \qquad (3.2.1)$$

The external transistor used is SQJA 00EP made by Vishay Siliconix, with $R_{DS(ON)}$ = 10,5 mΩ, a $V_{DS(MAX)}$ = 60 V and a gate charge Qg = 20 nC, C_{RSS} = 28 pF.

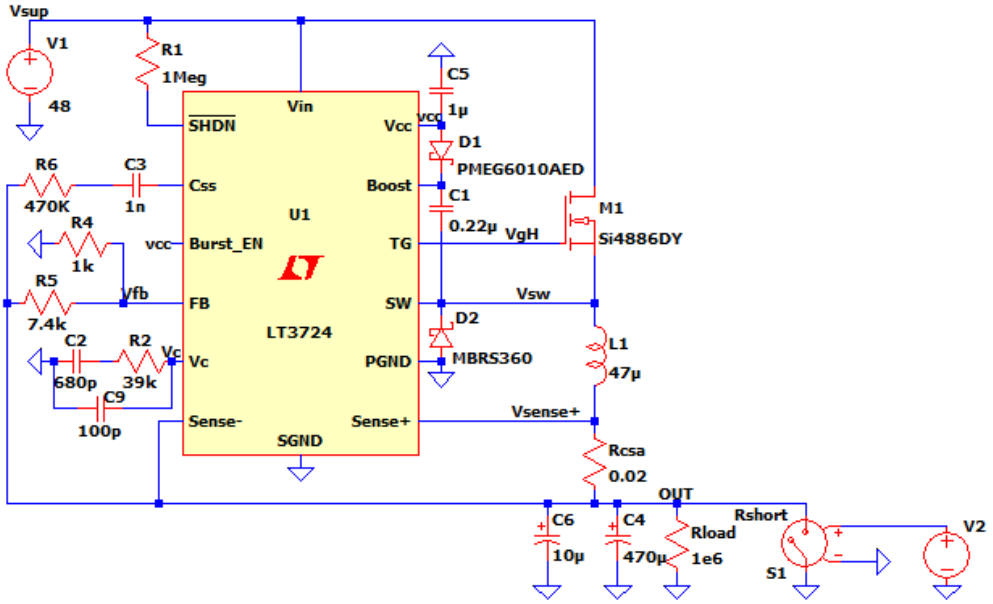

Figure 3.2.1. *LT 3724 buck converter simulation schematic*

Maximum power lost by conduction P_{COND} can be calculated with eq (3.2.3). and maximum power lost on transitions P_{TRAN} with (3.2.2) while the dissipated power by the external mosfet is their sum. So, P_{COND} = 0,37 W and P_{TRAN} = 0,1 W, in the end $P_{FET(TOTAL)}$ = 0,47 W.

$$P_{TRAN} = 2V_{IN}^2 \cdot I_{OUT(MAX)} \cdot C_{RSS} \cdot f_{SW} \qquad (3.2.2)$$

$$P_{COND} = \left(I_{OUT(MAX)}\right)^2 \cdot \frac{V_{OUT}}{V_{IN}} \cdot R_{DS(ON)} \qquad (3.2.3)$$

Inductor current error amplifier correct working test was done by applying a fast short-circuit at the output of the convertor, so in this way it can be observed the control loop stability.

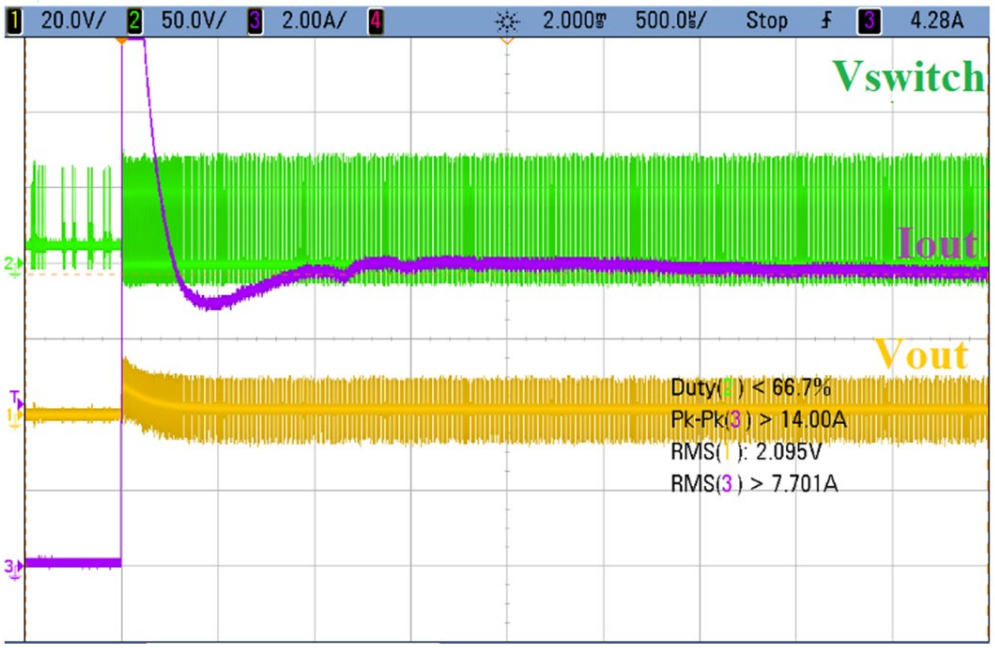

Figure 3.2.3. *Short -circuit aplied to the prototype converter built with LT 3724*

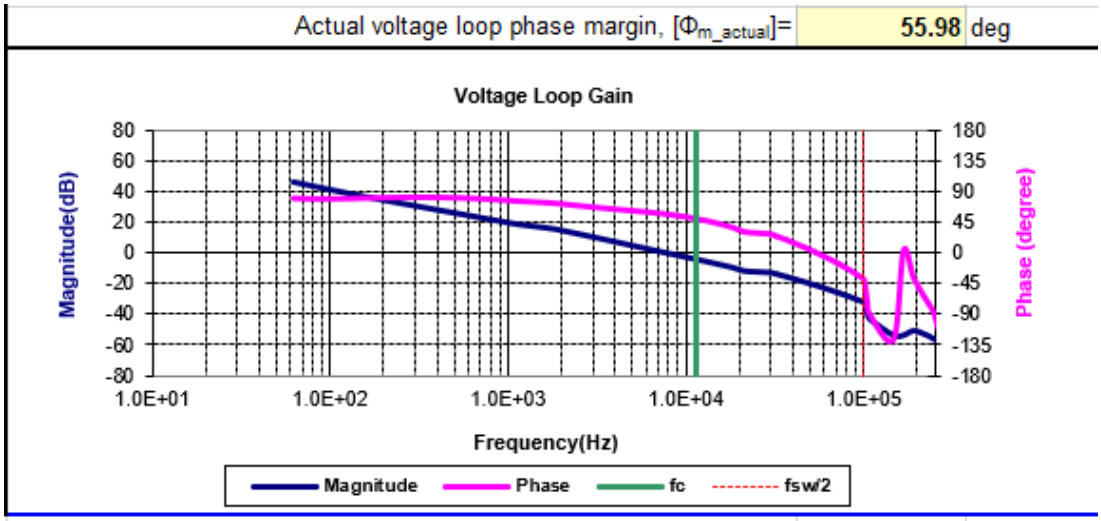

Figure 3.2.6. *Bode plot associated to the output voltage control loop Vout = 30 V and Iout= 4 A (simulation)*

After all the calculations and the SPICE simulation of the output voltage control loop in the situation where the converter works in CCM mode, the programmed output voltage is Vout = 30 V and load current has about 4 A, the bode plot is presented in figure 3.2.6. In order to test the prototype in the lab in the same conditions I've used a Bode analyzer built by Omicron Lab [31]. The result is in figure 3.2.7.

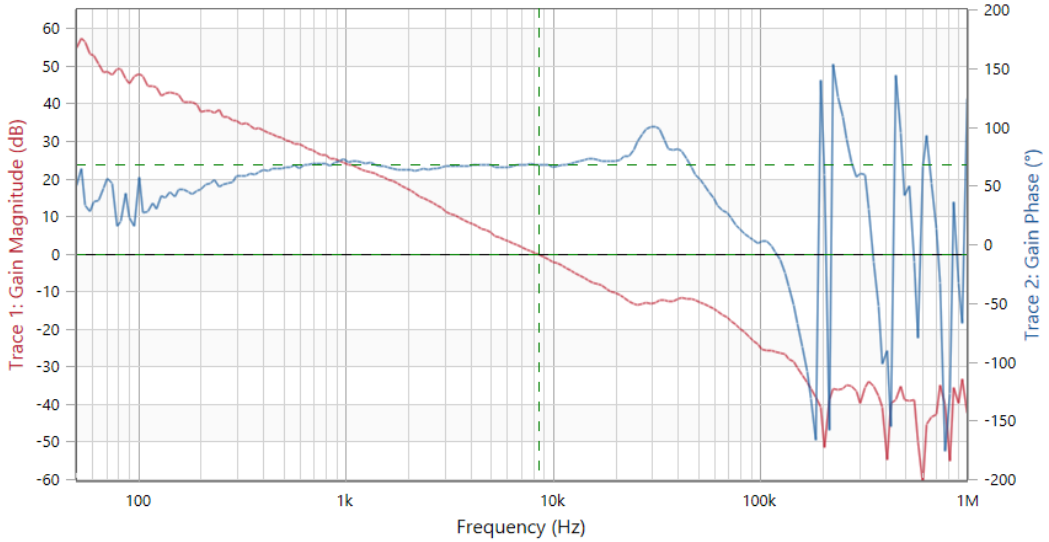

Figure 3.2.7. *Output voltage control loop Bode plot for Vout = 30 V and Iout = 4 A (prototype).*

Table 3.2.1*. Evolution and prototype enhancements [32]*		
	Type of the converter	
	LT3724 - CMC	Histeretic – subcap. 2.3
Output voltage range [V]	1,25 ÷ 40	0 ÷ 30
Output current range [A]	7,5	3
Output voltage ripple [mV]	15	120
PCB area [cm^2]	57,7	137,5
Convertor efficiency at power levels ≥90W.	94,2%	92,6%

Output voltage value is given by eq. (3.2.5).

$$R_{VOUT_{FB}} = R_{VAR_{I2C}}\left(\frac{V_{OUT}}{1.231} - 1\right) \qquad (3.2.5)$$

For a fast and easy control of the module I've used an I2C portable debugger [34].

3.3 Current mode buck converter design with synchronous rectification

A synchronous rectifier converter has the advange of a higher efficiency. In order to aim for a higher efficency I've started to design a convertor with synchronous rectifier using LT 3800. [35] [36]

The transistor used as an active diode should offer a lower R_{DSON}. SQJA 06EP [37] has an R_{DSON} = 8,7 mΩ and a current capability I_{D_MAX} = 57 A.

Considering V_{OUT} = 2V for $V_{IN(MAX)}$ = 50 V and $I_{OUT(MAX)}$ = 10 A will get the disipated power by the actiove diode $P_{LOW\_side\_cond}$ = 0,84 W while for 40 V at the

output lowers down to 0,18 W. C_{RSS} = 40 pF leads to higher losses during the device transitions, about 256 mW.

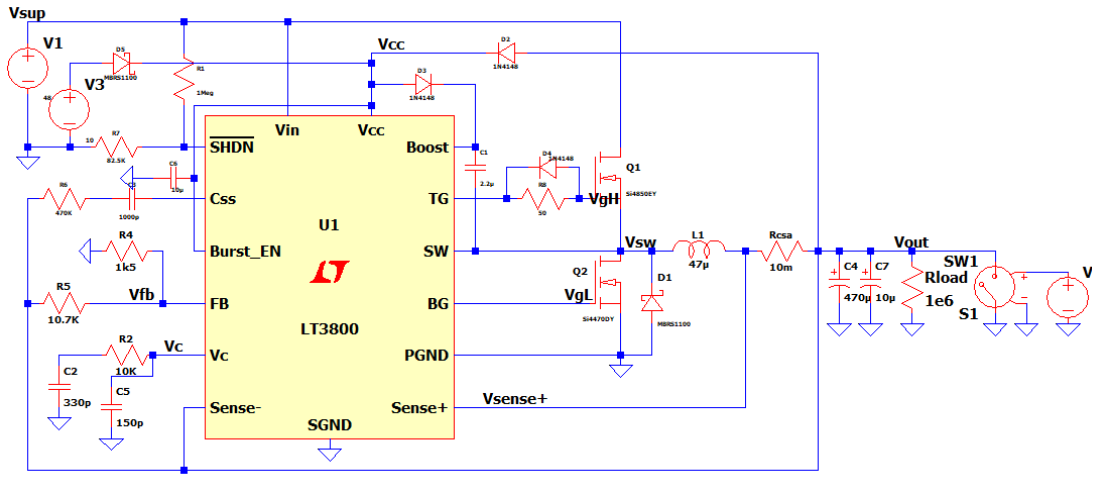

Figure 3.3.1. *Simulation of the concept schematic of the converter with LT3800*

Chapter 4

Vacuum tubes SPICE model coeficients computation

In order to obtain SPICE models coefficients of a certain electronic device, it is needed a good characterization of that device.

In the past the coefficients extraction was done by using datasheets numbers of the vacuum tubes or successive measurements without going over maximum allowed power of the device under test.

4.1 Vacuum tubes basic SPICE model equations

SPICE models of the triodes and tetrodes or pentodes became more popular during the last decade because the tubes are used more and more into the audio frequency amplifiers for auditions or musical instruments.

These SPICE models are based on identifying of some mathematic regressions that can fit better on the output characteristics shapes of the vacuum tubes.

SPICE models for tubes have been defined during the `90s, one of the pioneers being Scott Reynolds [38], based on the Child-Langmuir law, an exponential of 3/2, defining the anode current through a diode like this:

$$I_a = \frac{1}{k} V_a^{3/2} \tag{4.1.1}$$

This ideal law is valid for a perfectly symmetrical spatial charge zone. For a triode it looks like this:

$$I_a = \frac{1}{k_{G1}} (V_g + \frac{V_a}{\mu})^{3/2} \tag{4.1.2}$$

(4.1.2) is valid for:

$$V_g + \frac{V_a}{\mu} \geq 0 \text{ , otherwise } I_a = 0. \tag{4.1.3}$$

In practice tube's geometry is not perfectly cylindrical, for example the cathode has many times a rectangular shape and the grids are placed like a helix while the anode almost never is a perfect cylinder. [39]

Norman Koren replaces the tube with a voltage controlled current source. [41]

$$E_1 = \frac{V_a}{k_P} log\left[1 + e^{k_p\left(\frac{1}{\mu} + \frac{V_g}{\sqrt{k_{VB}+V_a^2}}\right)}\right] \quad (4.1.5)$$

$$I_a = \frac{E_1^X}{2k_{G1}}\left(1 + sgn(E_1)\right) \quad (4.1.6)$$

He used that $log\left(1 + exp(x)\right)$ =1 for $x \gg 1$ or 0 for $x \ll 1$ and $sgn(x) = 1$ for $x \geq 0$ or $sgn(x) = -1$ for $x < 0$. In this way the anode current I_a is always positive for positive U_a voltages and current flow is stopped for $E_1 < 0$.

4.2 Triode SPICE model coeficients computation

For this case study I have used a triode E188C(C) made by Philips. I(V) characteristic set of curves were lifted with the help of CCtracer, these can be seen in figure 4.2.2. SPICE model coefficients computation was done using a Java script [42]. Coefficients of the mode developed by N. Koren [41] can be computed in an easy way using the Java script developed by D. Nizhegorodov [43].

Table 4.2.1. *Triode SPICE model associated netlist[41]*

```
„.SUBCKT E188CC_TRIO 1 2 3 ; Anod Grid Cathode
+ PARAMS: CCG=...  CGP=...  CCP=...  RGI=... MU=... KG1=...KP=...
KVB=... VCT=... EX=...
E1 7 0
VALUE={V(1,3)/KP*LOG(1+EXP(KP*(1/MU+(VCT+V(2,3))/SQRT(KVB+V(1,
3)*V(1,3)))))}
RE1 7 0 1G ;
G1 1 3 VALUE={(PWR(V(7),EX)+PWRS(V(7),EX))/KG1}
RCP 1 3 1G ;
C1 2 3 {CCG} ;
C2 2 1 {CGP} ;
C3 1 3 {CCP} ;
D3 5 3 DX ;
R1 2 5 {RGI} ;
.MODEL DX D(IS=1N RS=1 CJO=10PF TT=1N)
.ENDS” [41]
```

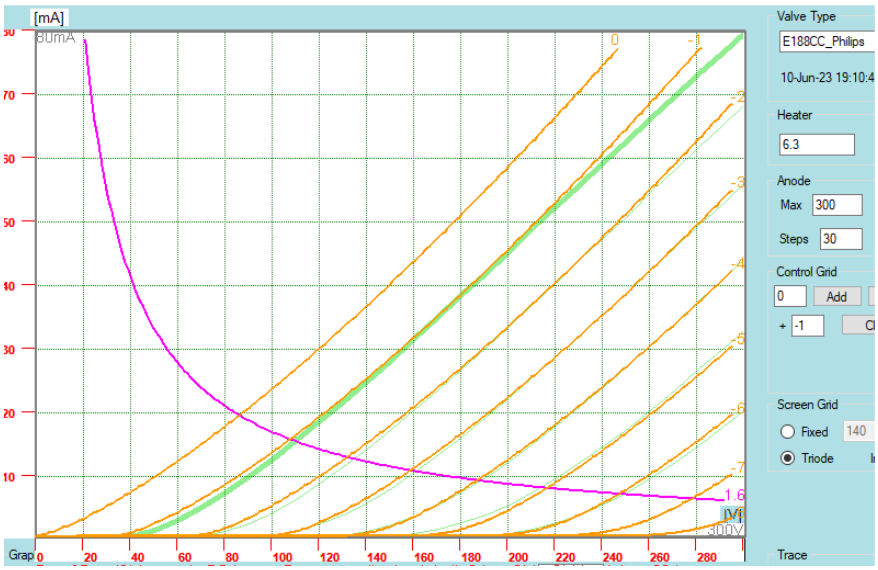

Figure 4.2.3. *Overlapping SPICE model characteristics with the ones of the device under test*

Table 4.2.2*. SPICE model coefficients associated to a triode E188C(C)*
CCG=0.05P CGP=1.4P CCP=0.5P RGI=2000 **+ MU=34.65 KG1=351.39 KP=763.7 KVB=2.1 VCT=0.00261 EX=1.33** * Vp_MAX=300 Ip_MAX=80 Vg_step=1 Vg_start=-1 Vg_count=6

SPICE model coefficients [41] in the table 4.2.1 generated after processing the results from figure 4.2.1 are presented in table 4.2.2.

Introducing this model in SPICE simulation where will be plotted the same characteristics like in figure 4.2.1, by overlapping the images of the two sets of results we can observe the accuracy of the SPICE model compared to the measurements done previously with CCtracer.

Chapter 5

Conclusions

5.1 Obtained results

During this thesis there was presented a series of contributions in the field of integrated testing systems for electronic components and devices.

In the **2nd chapter** were presented the steps followed during the development of an innovative integrated system of pulse testing for electronic tubes and other electronic components passive or active.

Chapter 2 starts with the design of the first modules that became part of CCTracer, these modules were developed from scratch, starting from concept definition phase, with simulations and validations for them followed by electrical schematics design.

During mechanical development I have built the printed circuit board for each module, then populated them with electronic components and in the end testing, measuring and debug them in the lab. The next step was their grouping and their interconnection to build up the curve tracer prototype CCTracer. This curve trace can work between 0 ÷ 400V with a peak current in a pulse of maximum 1 A.

During the **3rd chapter** it is detailed the upgrade of the heater power supply. Main improvements were done by raising the power, reducing the noise and slightly reducing the area. Afterwards the total energy efficiency has been raised with about 2 %.

In the **4th chapter** using CCTracer prototype, there were measured a few vacuum tubes and saved all the data in order to generate new sets of SPICE models coefficients.

5.2 Original contributions

- Development and evaluation up to prototype level of a system that measures the static characteristics of electronic tubes. [3,4].
- Developing a simple measurement solution for the current flowing through a device by level shifting the analog ground compared to the digital ground. [3].
- Partial integration into the control and command system of CCTracer of the concept used for the demo board with power management circuitry. [6]
- Development of a high efficiency heater power supply. (aprox. 96 %)[1,2]
- Computing a bunch of SPICE model coefficients associated to some electronic tubes used in the present in the power audio frequency amplifiers. [3,7].

5.3 List of original publications

1. **C. A. Iordache**, M. Bodea, „Analysis and design of a high efficiency current mode buck converter with I2C controlled output voltage," ***Romanian Journal*** *of Information Science and Technology (ROMJIST),* vol. 23, nr. No.2, pp. 188-203, 2020. **NumberWOS:000532321500006**.
2. **C.A. Iordache**, M. Bodea, „Analysis and design of a current mode buck converter with digitally controlled output voltage," *2019 International Semiconductor Conference (CAS),* nr. DOI: 10.1109/SMICND.2019.8923781,

pp. 309-312, 2019. **BEST PAPER AWARD:** SESSION SEMICONDUCTOR DEVICES AND ICs. **NumberWOS:000514295300065**

3. **C. A. Iordache**, C. Grecu and M. Bodea, „Computer Controlled Unit for Electronic Devices Characterization," *International Symposium ELMAR,* nr. DOI: 10.1109/ELMAR.2016.7731757. – CCTracer, pp. 73-76, 2015. **NumberWOS:000390949200017**
4. **C.A. Iordache**, C. Grecu, M. Bodea, „Variable regulated high voltage power supply," *International Symposium on Fundamentals of Electrical Engineering,* pp. 1-6, 2016. INSPEC Accession Number: 16563013, DOI: 10.1109/ISFEE.2016.7803163, ISBN:978-1-4673-9576-2 **NumberWOS:000392434400015**
5. C. Grecu, **C. A. Iordache**, „Portable I2C monitor and debugger," *2015 IEEE 21st International Symposium for Design and Technology in Electronic Packaging (SIITME),* Oct. 2015, **DOI: 10.1109/SIITME.2015.7342310**, Electronic ISBN:978-1-5090-0332-7 **NumberWOS:000377765500022**
6. C. Grecu., M. Bodea, **C. Iordache**, B. Istrate, „Bidirectional predicting zero cross detector for battery charger," *International Semiconductor Conference (CAS), Sinaia, Romania,* nr. 2017, pp. 293-296, 2017, DOI: 10.1109/SMICND.2017.8101229, ISBN:978-1-5090-3986-9. **BEST STUDENT PAPER AWARD**. **NumberWOS:000425844500065**
7. **C. A. Iordache** - 5 rapoarte științifice 2014-2017 SDETTIB

5.4 Perspectives for further developments

CCTracer architecture developed and presented in this thesis can be improved by introducing some Hall[4.] sensors to allow isolated current measurements. This will improve also the protection of the user regarding his electro security risks

I2C isolators could be integrated the same as in the variable high voltage power supply [4.] which will contribute to the safety of the operator. The circuits connected on the communication bus could be protected better in case of a damage.

In order to isolate better the computer ground which connects to CCTracer it can be added an isolation circuit for the USB up to 1 kV.

Raising the resolution of the characteristics measured by CCTracer can be done by using some analog to digital and digital to analog converters with a higher bit number. Also, this modification will need a higher computing power and maybe higher communication speeds.

The resolution and complexity of SPICE models can be raised in order to improve the tubes characterization, also the section of coefficients extraction can be implemented inside the Windows program so as in the end besides the CSV file with the data to have the possibility to export the entire SPICE model directly to the simulation virtual environments.

Bibliography

[3] J. E. Gorham, „Electron Tubes in World War II," *Proceedings of the IRE, vol. 35, no. 3, pp. 295-301,* March 1947.

[6] IEEE Standard Digital Interface for Programmable Instrumentation, „ANSI/IEEE Std 488-1978," *Revision of ANSI/IEEE 488-1975. Includes supplement IEEE Std 488A-19801,* nr. doi: 10.1109/IEEESTD.1978.7425098, pp. 1-84, 30 Nov. 1978.

[7] I. LXI Consortium, „Introducing LXI to your Network," LXI Consortium, Inc., 2013. [Interactiv]. Available: https://www.lxistandard.org/GuidesForUsingLXI/Introducing%20LXI%20To%20Your%20Network%20Administrator%20May%2024_2013.pdf.

[8] J. Ryland, „Can LXI replace GPIB?," *IEEE Autotestcon 2005,* pp. 739-743, 2005.

[9] K. M. B. Stasonis, „Choosing the Right Platform for Switching: PXI, USB or LXI?," *IEEE AUTOTESTCON, 2018, pp. 1-3, 2018..*

[14] M. Bodea, "Tuburile electronice", Ed. Tehnică, 1970.

[15] C. A. Iordache, C. Grecu and M. Bodea, „Computer Controlled Unit for Electronic Devices Characterization," *International Symposium ELMAR,* nr. doi: 10.1109/ELMAR.2016.7731757. – CCTracer, pp. 73-76, 2015.

[18] C. Grecu, „Contribuții la circuite de management al puterii," în *Teză de doctorat*, Bucharest, SDETTIB, 2017, p. cap.5.

[21] Microchip, „PIC18F25J50 Datasheet 28/44-Pin, Low-Power, High Performance USB Microcontrollers with nanoWatt XLP Technology," Microchip, 2011. [Interactiv]. Available: https://ww1.microchip.com/downloads/aemDocuments/documents/OTH/ProductDocuments/DataSheets/39931d.pdf. [Accesat 2023].

[24] Philips, „E188CC," *Philips Data Handbook,* pp. 1-10, 1969.

[25] K. S. K.S. Amitt, „A Unified Framework for Analysis and Design of a Digitally Current-Mode Controlled Buck Converter," *IEEE Transactions on Circuits and Systems I: Regular Papers,* vol. 63, nr. 11, pp. 2098 - 2107, Sept 2016.

[26] C.-J. H. Y.-S. Lee, „High Accuracy CMOS Current Sensing Circuit for Current Mode Control Buck Converter," *7th International Conference on Power Electronics and Drive Systems,* April 2007.

[28] Linear Technologies, „LT3724 High voltage current mode switching regulator controller," Analog Devices/, [Interactiv]. Available: https://www.analog.com/media/en/technical-documentation/data-sheets/3724fd.pdf [online]. [Accesat 2023].

[29] Würth Elektronik, „WE-HCI SMT High Current Inductor 74435584700," Würth Elektronik, [Interactiv]. Available: https://katalog.we-online.de/pbs/datasheet/74435584700.pdf [online]. [Accesat 2019].

[31] Omicron Lab, „Vector Network Analyzer - Bode 100," Omicron Lab, [Interactiv]. Available: https://www.omicron-lab.com/products/vector-network-analysis/bode-100 [online]. [Accesat 2023].

[32] C.A. Iordache, M. Bodea, „Analysis and design of a current mode buck converter with digitally controlled output voltage," *2019 International Semiconductor Conference (CAS),* nr. DOI: 10.1109/SMICND.2019.8923781, pp. 309-312, 2019.

[34] C. Grecu, C.A. Iordache, „Portable I2C monitor and debugger," *2015 IEEE 21st International Symposium for Design and Technology in Electronic Packaging (SIITME),* Oct. 2015.

[35] C. A. Iordache, M. Bodea, „Analysis and design of a high efficiency current mode buck converter with I2C controlled output voltage," *Romanian Journal of Information Science and Technology (ROMJIST),* vol. 23, nr. No.2, pp. 188-203, 2020.

[36] Analog Devices, „LT3800 High-Voltage Synchronous Current Mode Step-Down Controller," Linear Technologies, 2005. [Interactiv]. Available: https://www.analog.com/media/en/technical-documentation/data-sheets/3800fc.pdf [online]. [Accesat 2023].

[38] S. Reynolds, „Vacuum Tube Models for PSPICE Simulations," *Glass Audio,* nr. Nr.4, 1993.

[39] T. Tănăsescu, "Manual de tuburi și circuite electronice - Vol.1", București: Editura Academiei Republicii Populare Romîne, 1955.

[41] N. L. Koren, „Improved vacuum tube models for SPICE simulations," *[online], http://www.normankoren.com/Audio/Tubemodspice_article.html,* 2003.

[42] Wikipedia, „Java (programming language)," Oracle, [Interactiv]. Available: https://en.wikipedia.org/wiki/Java_(programming_language). [Accesat 2023].

[43] D. Nizhegorodov, „Model Paint Tools: Trace Tube Parameters over Plate Curves, Interactively," [Interactiv]. Available: https://www.dmitrynizh.com/tubeparams_image.htm. [Accesat 2023].